Int. J. Appl. Math. Comput. Sci., 2021, Vol. 31, No. 2, 233–245
DOI: 10.34768/amcs-2021-0016

A MIXED TYPE BOUNDARY–VALUE PROBLEM RELATED TO THE ELECTROSTATICS OF COLD PLASMA JET REACTORS BASED ON DIELECTRIC BARRIER DISCHARGE

PANAYIOTIS VAFEAS [a,*], POLYCARPOS K. PAPADOPOULOS [b], PANAGIOTIS SVARNAS [c]

[a]Department of Chemical Engineering
University of Patras
University Campus, 26504 Patras, Greece
e-mail: vafeas@chemeng.upatras.gr

[b]Department of Mechanical Engineering and Aeronautics
University of Patras
University Campus, 26504 Patras, Greece

[c]Department of Electrical and Computer Engineering
University of Patras
University Campus, 26504 Patras, Greece

A semi-analytical model is presented for the determination of the electric field in reactors used for cold atmospheric pressure plasma (CAPP) jet production, based on the concept of dielectric barrier discharge (DBD). These systems are associated with various applications in contemporary engineering, ranging from material processing to biomedicine, and at the same time they provide many challenges for fundamental research. Here, we consider a simplified system configuration of a single driven electrode, surrounding a thin dielectric tube, which does not contribute to the electric field, since the potential variation is immediate due to its negligible size. By employing the cylindrical coordinate system that perfectly fits the present plasma jet reactor, we separate the area of electric activity into three distinct domains according to the imposed external conditions, while our analysis is restricted to the electrostatic limit of Maxwell's equations. To this end, cylindrical harmonic field expansions are used for the potential, which produce the corresponding electric fields in each subdomain. Due to the imposed mixed-type boundary value problem, additional linear terms are incorporated, leading to three possible analytical solutions of the physical problem under consideration. The efficiency of the method is demonstrated by comparing the final formulae with a numerical solution, followed by the relevant discussion.

Keywords: DBD, cold plasma jet, reactor, mixed-type boundary-value problem, electrostatic potential theory.

1. Introduction

Problems in electrostatics, such as the limits of Maxwell's equations (Jackson, 1998), stand in the frontline of scientific research in engineering and modern technology, while they have always been a fertile ground for the formulation of new mathematical solutions. The need to calculate the electric field in engineering applications has generated interest in exploring mathematical techniques and combining different approaches in order to provide solutions for different geometries and in various coordinate systems. Before the computer revolution that has occurred in the past few decades, analytical solutions were the only means of obtaining information on the electric fields occurring in engineering applications. This is reflected in the vast effort that has been put into producing analytical solutions of the electrostatic field, by solving various boundary-value and mixed-type boundary-value problems in complex geometries (Sneddon, 1966). This painstaking effort of producing purely analytical solutions is still necessary, as the need for a stable and secure mathematical basis becomes the starting point of numerical coding for

*Corresponding author

tackling such problems.

The potential of mathematical solutions, however, should not be underestimated. The combination of mathematical techniques with numerical methods can give new semi-analytical approaches that allow us to harness the best of both parts. This is the motivation behind the construct work, which endeavors to present a semi-analytical solution for a mixed-type boundary value-problem, which is encountered in physical situations of cold atmospheric pressure plasma (CAPP) jet reactors based on the concept of the dielectric barrier discharge (DBD).

The principles of such CAPP jets and the related applications could be considered one of the most interdisciplinary scientific topics. In our other works, we deal with conjugated electro-hydrodynamic effects governed by the local electric field (Papadopoulos *et al.*, 2019; 2014; Logothetis *et al.*, 2016; Svarnas *et al.*, 2014), thermal effects strongly dependent on the externally applied electrical parameters (Svarnas *et al.*, 2018b), guided ionization waves propagating with ultrasonic velocities under the influence of time-varying electric fields (Svarnas *et al.*, 2018a; Gkelios *et al.*, 2011; Clément *et al.*, 2011; Gazeli *et al.*, 2013), chemical effects due to neutral and charged reactive species formation under complicated kinetics (Popov *et al.*, 2019), radiation over a wide range of the electromagnetic spectrum (Gazeli *et al.*, 2015), etc. This highly reactive medium is exploited by the employment of CAPP jets in state-of-the-art applications, like plasma biomedicine (Athanasopoulos *et al.*, 2019; 2018; Svarnas *et al.*, 2019; 2015; 2012). The ignition of the above plasmas and the subsequent evolution of main parameters are strongly dependent on the externally applied field, i.e., on the electrode configuration and the biasing potential. Thus, the resolution of the electric field in a CAPP jet reactor is crucial for the determination of the operational window of the equipment and the estimation of the involved plasma parameters.

The scope of this work is to present a semi-analytical solution for a mixed-type boundary-value problem that is encountered in CAPP jet reactors. The analytical approach is based on the separation-of-variables technique (Moon and Spencer, 1971); however, it is found that linear terms that satisfy Laplace's equation play a significant role in the analysis. The semi-analytical solution provides us a suitable representation of the electrostatic potential in terms of cylindrical harmonic eigenfunctions (Hobson, 1965), which is compared to a reference, purely numerical solution, offering a significant correction with respect to a first attempt (Vafeas *et al.*, 2020) to obtain such closed-form solutions. The comparison enables the determination of the final form of the semi-analytical solution and gives useful information on the behavior of the different parts of the solution, namely, the exponential, the constant and the linear part. It is to this end the effectiveness of the combination of applied mathematics and computer science is employed (see, e.g., Rabenstein and Trautmann, 2003; Maksimov and Mordukhovich, 2017; Gugat and Wintergerst, 2018; Bartecki, 2020).

2. Electrostatic problem development

We formulate the described physical problem of the electrostatic potential activity within the plasma jet reactor by virtue of the circular cylinder geometry (Moon and Spencer, 1971), given via the coordinates $\rho \in [0, +\infty)$, $\varphi \in [0, 2\pi)$ and $z \in (-\infty, +\infty)$ as

$$\mathbf{r} = \sum_{i=1}^{3} x_i \hat{\mathbf{x}}_i = z\,\hat{\mathbf{x}}_1 + \rho\cos\varphi\hat{\mathbf{x}}_2 + \rho\sin\varphi\hat{\mathbf{x}}_3, \quad (1)$$

in terms of the Cartesian basis $\hat{\mathbf{x}}_k$, $k = 1, 2, 3$ which defines a clockwise orthogonal system (ρ, φ, z). In this respect, we separate the DBD plasma jet reactor accordingly into subsectors as shown in Fig. 1.

The z-axis coincides with the symmetry axis of the plasma system, while the axis of the ρ-variable intersects the reactor vertically for any $\varphi \in [0, 2\pi)$. Therein, z_l is the length of the electrode, associated with a constant potential field V_e, which is attached to a thin, as readily assumed, dielectric tube at $\rho = \rho_0$ that does not contribute to the field distribution, being a fair approximation to the forthcoming analysis. Therein, the area of electrostatic interest is extended up to $z = z_r$, close to the exit of the jet, while moving towards $z \to +\infty$, far from the nozzle, and for any $\rho \in [0, \rho_0]$, there is no electrostatic activity, leading gradually to a zero potential, thus to a zero electric field.

Hence, assuming the negligible impingement that the dielectric tube has on the field distribution in the current model, the electrode attains a direct effect upon the working gas flow at $\rho = \rho_0$ due to the presence of the conditions applied on the boundary. Consequently, the three distinct areas of electrostatic activity in the gaseous

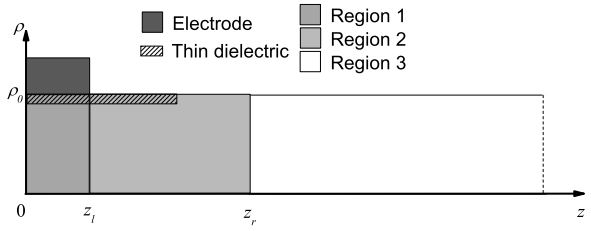

Fig. 1. Geometry of the plasma jet reactor, surrounded by gas and distinguished areas of electrostatic activity.

phase, being demonstrated in Fig. 1, are

$$\Omega_1 = \left\{\mathbf{r} \in \mathbb{R}^3 : \rho \in (0, \rho_0), \varphi \in [0, 2\pi), z \in (0, z_l)\right\}, \quad (2)$$

$$\Omega_2 = \left\{\mathbf{r} \in \mathbb{R}^3 : \rho \in (0, \rho_0), \varphi \in [0, 2\pi), z \in (z_l, z_r)\right\}, \quad (3)$$

$$\Omega_3 = \left\{\mathbf{r} \in \mathbb{R}^3 : \rho \in (0, \rho_0), \varphi \in [0, 2\pi), z \in (z_r, +\infty)\right\}. \quad (4)$$

Using the unit normal vectors of the coordinate system $\hat{\boldsymbol{\rho}}$, $\hat{\boldsymbol{\varphi}}$ and $\hat{\boldsymbol{z}}$ (Moon and Spencer, 1971; Hobson, 1965) , we introduce the gradient

$$\nabla = \hat{\boldsymbol{\rho}}\frac{\partial}{\partial \rho} + \frac{\hat{\boldsymbol{\varphi}}}{\rho}\frac{\partial}{\partial \varphi} + \hat{\boldsymbol{z}}\frac{\partial}{\partial z} \quad (5)$$

and the Laplacian

$$\Delta = \frac{1}{\rho}\frac{\partial}{\partial \rho}\left(\rho\frac{\partial}{\partial \rho}\right) + \frac{1}{\rho^2}\frac{\partial^2}{\partial \varphi^2} + \frac{\partial^2}{\partial z^2} \quad (6)$$

defined for any given $\rho \in [0, +\infty)$, $\varphi \in [0, 2\pi)$ and $z \in (-\infty, +\infty)$. Therefore, Maxwell's equations (Jackson, 1998) reduce to the electrostatic counterparts

$$\Delta V_j(\mathbf{r}) = 0, \quad j = 1, 2, 3, \quad (7)$$

since

$$\begin{aligned} \mathbf{E}_j(\mathbf{r}) &= -\nabla V_j(\mathbf{r}) \\ \nabla \cdot \mathbf{E}_j(\mathbf{r}) &= 0, \quad j = 1, 2, 3 \end{aligned} \quad (8)$$

for every $\mathbf{r} \in \Omega_j$, where V_j and $\mathbf{E}_j$ for $j = 1, 2, 3$ are the electrostatic potentials and electric fields corresponding to each area (2)–(4), respectively.

Our priority is to benefit from the rotational symmetry of the problem, due to its geometrical construction, the fact that leads to the exclusion of the angular dependence in any potential or electric field thereafter, providing the same solution in every half-plane that corresponds to the φ-variable. Thus, keeping the other two cylindrical variables $\rho \in [0, \rho_0]$ and $z \in [0, +\infty)$, according to the physical and mathematical development, the harmonic electrostatic potential fields retain azimuthal independence and are expressed by the series (Hobson, 1965)

$$\begin{aligned} V_1(\mathbf{r}) = {} & A_0^{(1)} z + B_0^{(1)} \\ & + \sum_{n=1}^{+\infty} J_0\left(\lambda_n^{(1)}\rho\right)\left[A_n^{(1)} e^{\lambda_n^{(1)} z} \right. \\ & \left. + B_n^{(1)} e^{-\lambda_n^{(1)} z}\right] \end{aligned} \quad (9)$$

for $\mathbf{r} \in \Omega_1$,

$$\begin{aligned} V_2(\mathbf{r}) = {} & A_0^{(2)} z + B_0^{(2)} \\ & + \sum_{n=1}^{+\infty} J_0\left(\lambda_n^{(2)}\rho\right)\left[A_n^{(2)} e^{\lambda_n^{(2)} z} \right. \\ & \left. + B_n^{(2)} e^{-\lambda_n^{(2)} z}\right] \end{aligned} \quad (10)$$

for $\mathbf{r} \in \Omega_2$ and

$$\begin{aligned} V_3(\mathbf{r}) = {} & A_0^{(3)} z + B_0^{(3)} \\ & + \sum_{n=1}^{+\infty} J_0\left(\lambda_n^{(3)}\rho\right)\left[A_n^{(3)} e^{\lambda_n^{(3)} z} \right. \\ & \left. + B_n^{(3)} e^{-\lambda_n^{(3)} z}\right] \end{aligned} \quad (11)$$

for $\mathbf{r} \in \Omega_3$, all written in terms of the Bessel functions of the zeroth order (Hobson, 1965), where the linear terms $A_0^{(j)} z + B_0^{(j)}$ for $j = 1, 2, 3$, incorporated within (9)–(11), define quantities that satisfy Laplace's equation *a priori* and play a crucial role in our forthcoming analysis, as an additional flexible factor that regulates the general expansion with respect to further validation via numerical implementation.

Obviously, similar linear terms concerning the other two remaining variables are not possible, due to the inability of the ρ-variable to satisfy Laplace's equation and due to the loss of the 2π-periodic property of the φ-variable, even though the latter does not contribute to the field calculation. Indeed, such terms are extremely important in mixed-type boundary-value problems (Sneddon, 1966), as it is the present status here, since each problem defines a unique physical case, wherein the analytical counterparts play a crucial role in the final solution. Besides, the effectiveness of the analytical formulae will be validated in the sequel via numerical elaboration. On the other hand, the linearly independent Neumann solutions (Hobson, 1965) are readily excluded from expansions (9)–(11), since they become singular for $\rho = 0$. The discrete parameters $\lambda_n^{(j)}$ for $j = 1, 2, 3$ with $n \geq 1$, coming from the method of separation of variables to Laplace's equation, along with the unknown constant coefficients $A_n^{(j)}$ and $B_n^{(j)}$ for any value of $j = 1, 2, 3$ and for $n \geq 0$, have to be calculated from the appropriate imposed boundary conditions that perfectly fit the particular physical problem.

In what follows, we analyze the nature of those conditions, beginning with the symmetry restrictions

$$\frac{\partial V_j(0, \varphi, z)}{\partial \rho} = 0, \quad j = 1, 2, 3 \quad \text{for } z \in [0, +\infty) \quad (12)$$

and

$$\frac{\partial V_1(\rho, \varphi, 0)}{\partial z} = 0 \quad \text{for } \rho \in [0, \rho_0], \quad (13)$$

which are applied on the symmetry axis of the problem for $\rho = 0$ and on the fictitious boundary at the beginning, as set, of our system for $z = 0$, respectively. At the exit of the plasma reactor and far away from the nozzle, the limit behaviour

$$\lim_{z\to+\infty} V_3(\rho,\varphi,z) = 0 \tag{14}$$

is required in order to secure the vanishing of the relative field, while around our system and at $\rho = \rho_0$ the physical analysis, described earlier in detail, demands the following fixed-type imposed boundary conditions:

$$V_1(\rho_0,\varphi,z) = V_e \qquad \text{for } z \in [0, z_l], \tag{15}$$

$$\frac{\partial V_2(\rho_0,\varphi,z)}{\partial \rho} = 0 \qquad \text{for } z \in [z_l, z_r], \tag{16}$$

$$V_3(\rho_0,\varphi,z) = 0 \qquad \text{for } z \in [z_r, +\infty), \tag{17}$$

being either of Dirichlet or Neumann type. Finally, standard continuity conditions between the common boundaries, in the absence of charges, are readily applied, initially at the intersection $z = z_l$, i.e.,

$$V_1(\rho,\varphi,z_l) = V_2(\rho,\varphi,z_l) \qquad \text{for } \rho \in [0,\rho_0], \tag{18}$$

$$\frac{\partial V_1(\rho,\varphi,z_l)}{\partial z} = \frac{\partial V_2(\rho,\varphi,z_l)}{\partial z} \qquad \text{for } \rho \in [0,\rho_0] \tag{19}$$

and secondary at $z = z_r$, that is,

$$V_2(\rho,\varphi,z_r) = V_3(\rho,\varphi,z_r) \qquad \text{for } \rho \in [0,\rho_0], \tag{20}$$

$$\frac{\partial V_2(\rho,\varphi,z_r)}{\partial z} = \frac{\partial V_3(\rho,\varphi,z_r)}{\partial z} \qquad \text{for } \rho \in [0,\rho_0]. \tag{21}$$

All the above formulations complete the introduction of a well-posed boundary-value problem in electrostatics.

3. Potentials in the plasma jet reactor

Primarily, the symmetry condition (12) is automatically satisfied with respect to the electrostatic potentials (9)–(11), since $J_0'(0) = -J_1(0) = 0$, according to the definition of Bessel's functions (Hobson, 1965). Proceeding, the limit condition (14), applied on the expansion (11), yields

$$A_0^{(3)} = B_0^{(3)} = 0, \quad A_n^{(3)} = 0, \quad n \geq 1. \tag{22}$$

Therefore, the electrostatic field (11) becomes

$$V_3(r) = \sum_{n=1}^{+\infty} B_n^{(3)} J_0\left(\lambda_n^{(3)}\rho\right) e^{-\lambda_n^{(3)} z} \quad \text{for } r \in \Omega_3. \tag{23}$$

In the sequel, the other symmetry condition (13), applied to the electrostatic potential (9), leads to

$$A_0^{(1)} + \sum_{n=1}^{+\infty} \lambda_n^{(1)} \left(A_n^{(1)} - B_n^{(1)}\right) J_0\left(\lambda_n^{(1)}\rho\right) = 0 \qquad \text{for } \rho \in [0,\rho_0], \tag{24}$$

which reveals that an acceptable solution is

$$A_0^{(1)} = 0 \text{ and } A_n^{(1)} - B_n^{(1)} = 0 \text{ or } B_n^{(1)} = A_n^{(1)} \qquad \text{with } n \geq 1 \tag{25}$$

and, therefore, the relative field (9) is rewritten as

$$V_1(r) = B_0^{(1)} + \sum_{n=1}^{+\infty} C_n^{(1)} J_0\left(\lambda_n^{(1)}\rho\right) \cosh\left(\lambda_n^{(1)} z\right) \qquad \text{for } r \in \Omega_1, \tag{26}$$

where $C_n^{(1)} \equiv 2A_n^{(1)}$ with $n \geq 1$ is the newly defined constant coefficient of the particular potential field. Next, we reinforce the prescribed boundary conditions (15)–(17) on the surroundings of the reactor to the potentials (26), (10) and (23), respectively. Hence we conclude with the corresponding relationships

$$B_0^{(1)} + \sum_{n=1}^{+\infty} C_n^{(1)} J_0\left(\lambda_n^{(1)}\rho_0\right) \cosh\left(\lambda_n^{(1)} z\right) = V_e \qquad \text{for } z \in [0, z_l], \tag{27}$$

$$\sum_{n=1}^{+\infty} J_0'\left(\lambda_n^{(2)}\rho_0\right) \left[A_n^{(2)} e^{\lambda_n^{(2)} z} + B_n^{(2)} e^{-\lambda_n^{(2)} z}\right] = 0 \qquad \text{for } z \in [z_l, z_r] \tag{28}$$

and

$$\sum_{n=1}^{+\infty} B_n^{(3)} J_0\left(\lambda_n^{(3)}\rho_0\right) e^{-\lambda_n^{(3)} z} = 0 \qquad \text{for } z \in [z_r, +\infty). \tag{29}$$

In order to manipulate Eqns. (27)–(29), we initially demand from (27) and without loss of generality that

$$B_0^{(1)} = V_e, \tag{30}$$

whilst in order to obtain non-trivial potential fields that are not zero and since $J_0'\left(\lambda_n^{(2)}\rho_0\right) = -J_1\left(\lambda_n^{(2)}\rho_0\right)$ we are obliged to evaluate accordingly the corresponding separation constants as

$$\lambda_n^{(1)} = \lambda_n^{(3)} = \frac{r_n}{\rho_0} \quad \text{and} \quad \lambda_n^{(2)} = \frac{s_n}{\rho_0} \quad \text{with } n \geq 1, \tag{31}$$

by virtue of the roots of Bessel's function of the zeroth (r_n) and first (s_n) order, meaning $J_0(r_n) = 0$ and $J_1(s_n) = 0$. Bearing in mind (30) and (31), the implicated potentials (26), (10) and (23) are herein given by the formulae

$$V_1(\mathbf{r}) = V_e + \frac{1}{2}\sum_{n=1}^{+\infty} D_n^{(1)} J_0\left(r_n\frac{\rho}{\rho_0}\right) \times \left(e^{r_n\frac{z-z_l}{\rho_0}} + e^{-r_n\frac{z+z_l}{\rho_0}}\right) \quad (32)$$

for $\mathbf{r} \in \Omega_1$,

$$V_2(\mathbf{r}) = A_0^{(2)} z + B_0^{(2)} + \sum_{n=1}^{+\infty} J_0\left(s_n\frac{\rho}{\rho_0}\right) \times \left[C_n^{(2)} e^{s_n\frac{z-z_r}{\rho_0}} + D_n^{(2)} e^{s_n\frac{z_l-z}{\rho_0}}\right] \quad (33)$$

for $\mathbf{r} \in \Omega_2$ and

$$V_3(r) = \sum_{n=1}^{+\infty} C_n^{(3)} J_0\left(r_n\frac{\rho}{\rho_0}\right) e^{r_n\frac{z_r-z}{\rho_0}}, \quad (34)$$

for $\mathbf{r} \in \Omega_3$, where the exponential modifications into (32)–(34) are a necessary step, made for future numerical issues, by denoting $D_n^{(1)} \equiv C_n^{(1)} \exp(r_n z_l/\rho_0)$, $C_n^{(2)} \equiv A_n^{(2)} \exp(s_n z_r/\rho_0)$, $D_n^{(2)} \equiv B_n^{(2)} \exp(-s_n z_l/\rho_0)$ and $C_n^{(3)} \equiv B_n^{(3)} \exp(-r_n z_r/\rho_0)$ for every $n \geq 1$ as the new constant coefficients that must be evaluated.

Concluding, we remain with the transmission conditions (18)–(21), which in terms of the fields (32)–(34) will provide us with the rest of the unknown constant coefficients. However, here we are obliged to make an important remark, concerning the potential field V_2 from (33), which contains the linear term $A_0^{(2)} z + B_0^{(2)}$. In order to demonstrate analytically and numerically how this term influences the final solution of the problem, we distinguish three separate cases that lead to three different possible solutions, namely, A, B and C. Solution A refers to the case where only the exponential terms are present ($A_0^{(2)} = B_0^{(2)} = 0$), solution B retains the constant term $B_0^{(2)} \neq 0$ ($A_0^{(2)} = 0$) and solution C assumes the existence of the full linear term ($A_0^{(2)} \neq 0$ and $B_0^{(2)} \neq 0$). For this purpose, we interfere with the transmission conditions (18)–(21), by writing the constant potential V_e as a series expansion in terms of Bessel eigensolutions (Hobson, 1965) via the expansion

$$V_e = 2V_e \sum_{n=1}^{+\infty} \frac{1}{r_n J_1(r_n)} J_0\left(r_n\frac{\rho}{\rho_0}\right) \quad \text{for any } \rho \in [0,\rho_0], \quad (35)$$

which actually comprises the Fourier–Bessel expansion of V_e. Moreover, since we have to work with different arguments of Bessel functions of zeroth order (see, for instance, (32)–(34)), we need to introduce the orthogonality relation

$$\int_0^{\rho_0} \rho J_0\left(r_n\frac{\rho}{\rho_0}\right) J_0\left(r_{n'}\frac{\rho}{\rho_0}\right) \mathrm{d}\rho = \delta_{nn'}\frac{[\rho_0 J_1(r_n)]^2}{2} \quad (36)$$

and the trivial integral

$$\int_0^{\rho_0} \rho J_0\left(s_n\frac{\rho}{\rho_0}\right) J_0\left(r_{n'}\frac{\rho}{\rho_0}\right) \mathrm{d}\rho = \frac{\rho_0^2 r_{n'} J_0(s_n) J_1(r_{n'})}{r_{n'}^2 - s_n^2} \quad (37)$$

with $n, n' \geq 1$. Therefore, we substitute the potential fields (32)–(34) within the transition conditions (18)–(21) for each of the three prementioned cases A, B and C with respect to the term $A_0^{(2)} z + B_0^{(2)}$, next we multiply both the sides of the obtained relations by $\rho J_0\left(r_{n'}\rho/\rho_0\right)$ for $n' \geq 1$, we integrate over the interval $[0,\rho_0]$ and we finally use (36) and (37), as well as the convenient notations

$$J_{n/n'} = \frac{2}{r_{n'}^2 - s_n^2}\frac{J_0(s_n)}{J_1(r_{n'})}, \quad V_{n'} = \frac{2V_e}{r_{n'} J_1(r_{n'})}, \quad (38)$$

and the exponential function

$$f(z\,; q_n) = \exp\left(q_n\frac{z}{\rho_0}\right), \quad (39)$$

where

$$q_n = \begin{cases} r_n, \\ s_n, \end{cases} \quad (40)$$

$n \geq 1$, so as to obtain the following relations for the coefficient:

Solution A $\left(A_0^{(2)} = B_0^{(2)} = 0\right)$:

$$\left[1 + f(-2z_l; r_{n'})\right] D_{n'}^{(1)} - - 2r_{n'} \sum_{n=1}^{+\infty} J_{n/n'} \left[f(z_l - z_r; s_n) C_n^{(2)} + D_n^{(2)}\right] = -2V_{n'}, \quad (41)$$

$$\left[1 - f(-2z_l; r_{n'})\right] D_{n'}^{(1)} - 2\sum_{n=1}^{+\infty} s_n J_{n/n'} \left[f(z_l - z_r; s_n) C_n^{(2)} - D_n^{(2)}\right] = 0, \quad (42)$$

$$r_{n'}\sum_{n=1}^{+\infty}J_{n/n'}\left[C_n^{(2)}+f\left(z_l-z_r;s_n\right)D_n^{(2)}\right]-C_{n'}^{(3)}=0 \quad (43)$$

and

$$\sum_{n=1}^{+\infty}s_nJ_{n/n'}\left[C_n^{(2)}-f\left(z_l-z_r;s_n\right)D_n^{(2)}\right]+C_{n'}^{(3)}=0, \quad (44)$$

with all the above for every value of $n'\geq 1$.

Solution B $\left(A_0^{(2)}=0 \text{ and } B_0^{(2)}=V_e\right)$:

$$\left[1+f\left(-2z_l;r_{n'}\right)\right]D_{n'}^{(1)}-2r_{n'}\sum_{n=1}^{+\infty}J_{n/n'}\left[f\left(z_l-z_r;s_n\right)C_n^{(2)}+D_n^{(2)}\right]=0, \quad (45)$$

$$\left[1-f\left(-2z_l;r_{n'}\right)\right]D_{n'}^{(1)}-2\sum_{n=1}^{+\infty}s_nJ_{n/n'}\left[f\left(z_l-z_r;s_n\right)C_n^{(2)}-D_n^{(2)}\right]=0, \quad (46)$$

$$r_{n'}\sum_{n=1}^{+\infty}J_{n/n'}\left[C_n^{(2)}+f\left(z_l-z_r;s_n\right)D_n^{(2)}\right]-C_{n'}^{(3)}=-V_{n'} \quad (47)$$

and

$$\sum_{n=1}^{+\infty}s_nJ_{n/n'}\left[C_n^{(2)}-f\left(z_l-z_r;s_n\right)D_n^{(2)}\right]+C_{n'}^{(3)}=0, \quad (48)$$

with all the above for every value of $n'\geq 1$.

Solution C $\left(A_0^{(2)}=-\frac{V_e}{z_r-z_l} \text{ and } B_0^{(2)}=z_r\frac{V_e}{z_r-z_l}\right)$:

$$\left[1+f\left(-2z_l;r_{n'}\right)\right]D_{n'}^{(1)}-2r_{n'}\sum_{n=1}^{+\infty}J_{n/n'}\left[f\left(z_l-z_r;s_n\right)C_n^{(2)}+D_n^{(2)}\right]=0, \quad (49)$$

$$\left[1-f\left(-2z_l;r_{n'}\right)\right]D_{n'}^{(1)}-2\sum_{n=1}^{+\infty}s_nJ_{n/n'}\left[f\left(z_l-z_r;s_n\right)C_n^{(2)}-D_n^{(2)}\right]=-\frac{2\rho_0V_{n'}}{r_{n'}\left(z_r-z_l\right)}, \quad (50)$$

$$r_{n'}\sum_{n=1}^{+\infty}J_{n/n'}\left[C_n^{(2)}+f\left(z_l-z_r;s_n\right)D_n^{(2)}\right]-C_{n'}^{(3)}=0 \quad (51)$$

and

$$\sum_{n=1}^{+\infty}s_nJ_{n/n'}\left[C_n^{(2)}-f\left(z_l-z_r;s_n\right)D_n^{(2)}\right]+C_{n'}^{(3)}=\frac{\rho_0V_{n'}}{r_{n'}\left(z_r-z_l\right)}, \quad (52)$$

with all the above for every value of $n'\geq 1$.

The systems of equations (41)–(44) (solution A), (45)–(48) (solution B) and (49)–(52) (solution C) stand for an infinite linear system of four sets of algebraic equations, including the four constant coefficients $D_{n'}^{(1)}$, $C_n^{(2)}$, $D_n^{(2)}$ and $C_{n'}^{(3)}$ with $n,n'\geq 1$, which is handled with cut-off techniques in order to obtain quadratic systems, whenever the number of sets $n'\geq 1$ of relations coincides with the number of terms $n\geq 1$ of the infinite series, by assuming a common upper limit $N\in\mathbb{N}^*$ so as to obtain the desired accuracy during the numerical implementation for the evaluation of the unknown constant coefficients. As a matter of fact, we have to take $n'=1,2,\ldots,N$ and $\sum_{n=1}^{+\infty}(\cdots)\simeq\sum_{n=1}^{N}(\cdots)$, concerning (41)–(44) (solution A), (45)–(48) (solution B) and (49)–(52) (solution C), whereas the controlled value N is conveniently regulated on the basis of convergence of the final results. Doing so, we have to solve systems of type 4×4, 8×8, ... ,$4N\times 4N$, thus, by the definition of $N\times N$ blocks of matrixes, each one of type 4×4, which form a total $4N\times 4N$ matrix $\mathbf{A}$ of the coefficients of the unknowns, as well as by means of the vector of the unknown coefficients $\mathbf{x}$ of type $4N\times 1$ and in view of the vector of the known constants $\mathbf{b}$ of the same type $4N\times 1$, the block of systems for each unique solution A, B or C can be written as

$$\mathbb{A}\,\mathbf{x}=\mathbf{b}\ \Rightarrow\ \mathbf{x}=\mathbb{A}^{-1}\mathbf{b} \quad (53)$$

for every $n=1,2,\ldots,N$ with $N\in\mathbb{N}^*$, since the determinant of $\mathbb{A}$ is proven to be nonzero, hence the inverse matrix exists. The linear system (53) yields the calculation of the constant coefficients $D_n^{(1)}$, $C_n^{(2)}$, $D_n^{(2)}$ and $C_n^{(3)}$ for $n=1,2,\ldots,N$, taking into account every supposed solution.

Once the unknowns are obtained, the three possible solutions A, B and C of the given electrostatic potential boundary value problem are rendered by

$$V_1(\mathbf{r})=V_e+\frac{1}{2}\sum_{n=1}^{+\infty}D_n^{(1)}J_0\left(r_n\frac{\rho}{\rho_0}\right)\left[f\left(z-z_l;r_n\right)+f\left(-z-z_l;r_n\right)\right] \quad (54)$$

for $\mathbf{r} \in \Omega_1$,

$$V_2(\mathbf{r}) = \begin{cases} 0, & \text{sol. A} \\ V_e, & \text{sol. B} \\ \frac{z_r - z}{z_r - z_l} V_e, & \text{sol. C} \end{cases} + \sum_{n=1}^{+\infty} J_0\left(s_n \frac{\rho}{\rho_0}\right) \left[C_n^{(2)} f(z - z_r; s_n) + D_n^{(2)} f(z_l - z; s_n) \right] \quad (55)$$

for $\mathbf{r} \in \Omega_2$ and

$$V_3(\mathbf{r}) = \sum_{n=1}^{+\infty} C_n^{(3)} J_0\left(r_n \frac{\rho}{\rho_0}\right) f(z_r - z; r_n) \quad (56)$$

for $\mathbf{r} \in \Omega_3$, provided the definition (40), while the inserted constant coefficients $D_n^{(1)}$, $C_n^{(2)}$, $D_n^{(2)}$ and $C_n^{(3)}$ with $n \geq 1$ are calculated for the different examined situations. Therein, the corresponding electric fields are computed by (8) in each region and for every solution A, B and C. Thus we end up with our model solution in CAPP jet reactor systems.

The final solution is a linear combination of solutions A, B and C. It is evident that the linear combination could have been expressed as a single parametric formulation, which would include the three main contributions, i.e., the linear term of solution C, the constant term of solution B and the series expansion, which is standard in all three solutions (see, for instance, the three different relationships in (54), while the other two potentials (54) and (56) retain one formation). The reason why we have chosen to present the above cumulative solution as three separate parts is that it is easier to understand their separate contributions. Besides, when dealing with such mixed-type boundary value problems, the choice of the associated eigenfunctions of the implied potentials becomes a very complicated task that depends each time on the particular problem and a trial-and-error technique is eventually inevitable (Sneddon, 1966).

4. Results and a discussion

The three solutions A, B and C that were presented in the previous section have different characteristics. Solution A is derived from a well-defined system where all the unknowns are unique. However, it includes the contribution only of the exponential terms and lacks any influence from the constant and the linear term, i.e., from the terms with the coefficients $A_0^{(2)}$ and $B_0^{(2)}$. On the other hand, solution B, which includes the contribution of the constant term, and solution C, which includes the contribution of both the constant and linear terms, are derived from systems that are over-determined by one and two variables, respectively. In terms of completeness, solution C is the best choice, as it incorporates all the contributions (exponential, constant and linear).

A sound mathematical procedure would be to keep solution C and try to determine the extra unknowns via a sensitivity analysis in conjunction with a reference numerical solution. The numerical solution, which is unique, can serve as a reference guide for the determination of the extra variables based on a variational procedure. However, this variational procedure is cumbersome and requires extensive try-and-error tests, because the variational parameters are arbitrary and their determination lacks physical intuition. In the present work, we follow a different path to reach the same result, by examining the forms of solutions A, B and C, and determining a linear combination of these solutions that fits the numerical reference solution. The result of this approach is equivalent to the one that would be obtained from the variational procedure of the sensitivity analysis, but it is obviously much easier to perform.

The numerical solution was obtained by solving the 3D problem (i.e., not taking advantage of the symmetry of the problem) on the OpenFOAM platform (Weller *et al*., 1998). The cylindrical domain was meshed using a standard butterfly-type grid. A grid sensitivity analysis that was conducted between two meshes, one with 522240 cells (normal mesh) and one with 661500 cells (dense mesh) revealed a maximum difference of 1.2% in the value of the potential. Therefore, the normal mesh size was employed in the computations, while a separate mesh with the above size was created for each of the cases considered in this study. Since the computational domain requires boundary conditions at finite distances, it was necessary to conduct numerical tests to determine the axial length of the cylindrical geometry that corresponds to the boundary condition (14). It was found that an axial distance of 100 radii was adequate to produce results independent of the axial length of the cylinder. Regarding the solution technique, Laplace's equation was solved using the finite volume method with a linear, second-order accurate discretization scheme.

Figure 2 shows the distributions of (a) the electric potential and (b) the axial component of the electric field, along the axis of the cylindrical geometry. Each figure includes the result of the numerical calculation, which serves as a reference solution, and the curves obtained from solutions A, B and C. It is evident that none of the three analytical solutions fit the numerical reference curve. This was expected taking account of the fact that solution A lacks the contribution of the constant and linear terms, while solutions B and C have approximations in the evaluation of the extra unknowns of their linear systems. However, each of the solutions has a distinct behaviour, which is more pronounced in the axial component of the electric field in Fig. 2(b).

It can be seen in Fig. 2(b) that solution A contributes

to the electric field mainly in the limit between Region 1, being inside the electrode, and Region 2, which is bounded with a Neumann boundary condition. Solution C contributes to the electric field in the core of Region 2, while solution B has its main contribution, in the limit between Regions 2 and 3, which is bounded with a Dirichlet boundary condition. Although none of the three curves fits the numerical reference curve, it is relatively easy to determine a linear combination of the three analytical solutions that will. It is evident that solution C will be the main contributor and solutions A and B will provide the corrections in the limits between the three regions. It was found that, for the specific geometrical characteristics, i.e., the electrode inner radius 0.4 cm, the electrode length 1 cm and the change between the Neumann and the Dirichlet boundary conditions at 4 cm from the origin, the coefficients for the linear combination are 0.3 for solution A, 0.03 for solution B and 0.94 for solution C. It can be seen from Figs. 2(a) and (b) that, with the specific linear combination of the three solutions, the electric potential and the axial component of the electric field fit perfectly the ones obtained from the numerical calculations.

Figure 3 shows contours of the electric potential and the axial and radial components of the electric field in a slice of the cylindrical domain, which extends along the radial direction from the origin to 0.2 cm and in the axial direction from the origin to 8 cm. The distribution of the electric potential is uniform along the radial direction and varies only axially. The variation is linear between the end of the electrode and the location where the Neumann condition changes to Dirichlet. In fact, the axial distribution of the electric potential at any given radius is similar to the one along the axis of symmetry, which is shown in Fig. 2(b). The radial electric field is non-zero only in the areas where there is an inter-change between the three regions. In detail, it is positive when close to the edge of the driven electrode and negative in the area where the Neumann condition changes to Dirichlet. Finally, the axial component of the electric field is almost constant in Region 2 and rapidly drops to zero as we move away from this region.

The second geometry that was studied had the same axial distances as the first case, but a different radius. Specifically, the second geometry has the electrode inner radius 0.2 cm, the electrode length 1 cm and the change between the Neumann and the Dirichlet boundary conditions is prescribed at 4 cm from the origin. Figures 4(a) and (b) depict the distribution of the electric potential and of the axial component of the electric field, for a geometry with half the radius, compared with the previous one. It is noted that the coefficients of the linear combination are not constant in the different cases, as they depend on the geometrical characteristics of the specific problem.

In general, the three analytical solutions display similar behaviors as in the first geometry, but with different magnitudes. It was determined that the coefficients of the linear combination that fits the reference numerical curve are 0.02 for solution A, 0.02 for solution B and 0.96 for solution C. The difference with the coefficients of the previous case is small and the overall solution is again dominated by the contribution of solution C.

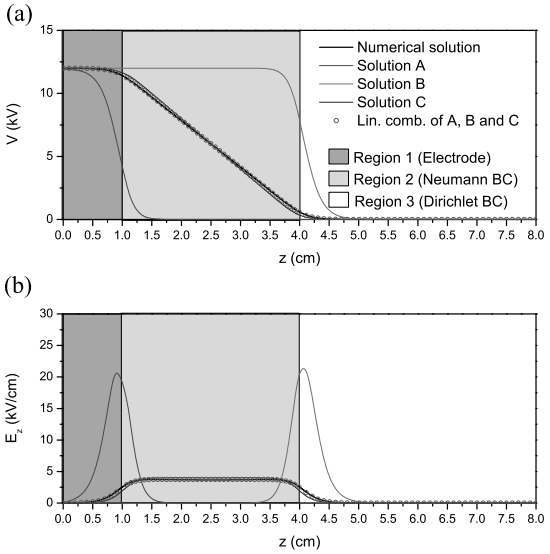

Fig. 2. Distribution of the electric potential (a) and the axial component of the electric field (b) along the axis of the cylindrical geometry. The electrode inner radius is 0.4 cm and its length is 1 cm. The change between the Neumann and the Dirichlet boundary conditions is prescribed at 4 cm from the origin.

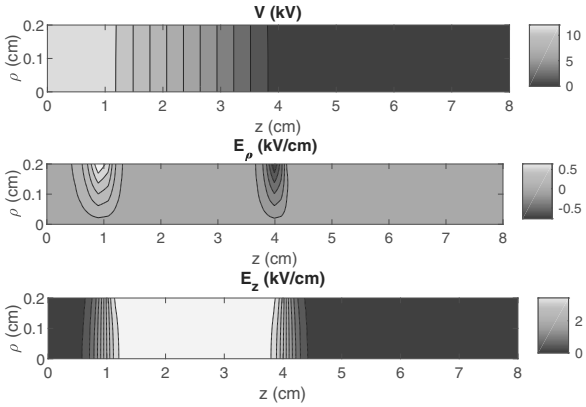

Fig. 3. Contours of the electric potential (a), the radial component of the electric field (b) and the axial component of the electric field (c). The electrode inner radius is 0.4 cm and its length is 1 cm. The change between the Neumann and the Dirichlet boundary conditions is prescribed at 4 cm from the origin.

The contours of the electric potential and the axial and radial components of the electric field in a slice of the cylindrical domain, which extends along the radial direction from the origin to 0.1 cm and in the axial direction from the origin to 8 cm, are shown in Fig. 5. As expected the plots reveal similar behaviors with the previous geometry for the three fields. The potential displays a linear drop from the maximum value to zero along Region 2, the radial electric field is active only in the inter-regional areas and the axial electric field is approximately constant in Region 2 and zero everywhere else. The magnitude of the components of the electric field is similar to the one in the previous geometry, despite the fact that now the radius is halved.

The third geometry that we examined has the same radial properties as the first one, i.e., the electrode inner radius is 0.4 cm, but the length is halved, i.e., the electrode length is 0.5 cm and the change between the Neumann and Dirichlet boundary conditions is prescribed at 2 cm from the origin. As shown in Figs. 6(a) and (b), in this case, solutions A and B contribute a slightly higher part to the overall solution. It was determined that the coefficients of the linear combination that fit the reference numerical curve are 0.05 for solution A, 0.05 for solution B and 0.9 for solution C.

Figure 7 shows contours of the electric potential and the axial and radial components of the electric field in a slice of the cylindrical domain, which extends along the radial direction from the origin to 0.2 cm and in the axial direction from the origin to 4 cm. A comparison with the previous results shows that in this case there is an observable variation in the fields in the radial direction. Although the general behaviour is similar, the areas around the inter-regional borders, where the changes in the radial and axial components of the electric field take place, are wider. Moreover, there is a significant increase in the magnitude of the electric field, as it is approximately doubled. This fact highlights the relative importance of the axial dimensions of the electrode compared with the radial ones.

Finally, Figs. 8 and 9 show the corresponding results for a geometry that has half all the distances with respect to the first one. In fact, it has similar axial properties to the third case, i.e., the length of the electrode is 0.5 cm and the change between the Neumann and Dirichlet boundary conditions is prescribed at 2 cm from the origin, but half its radius, that is, 0.2 cm.

The coefficients of the linear combination that fits the reference numerical curve in this case are 0.03 for solution A, 0.03 for solution B and 0.94 for solution C, which is similar to the first case. It is interesting to note that this is the same linear combination that fitted the first case, which indicates that, if the dimensions are proportional, the coefficients of solutions A, B and C are the same. To assess the validity of this conclusion, we tested an analogous case to the first geometry, where all the dimensions are reduced tenfold. The results for the distributions of the electric potential and the axial component of the electric field, along the axis of the cylindrical geometry, are shown in Fig. 10. The coefficients of the linear combination that fits the reference numerical curve are 0.03 for solution A, 0.03

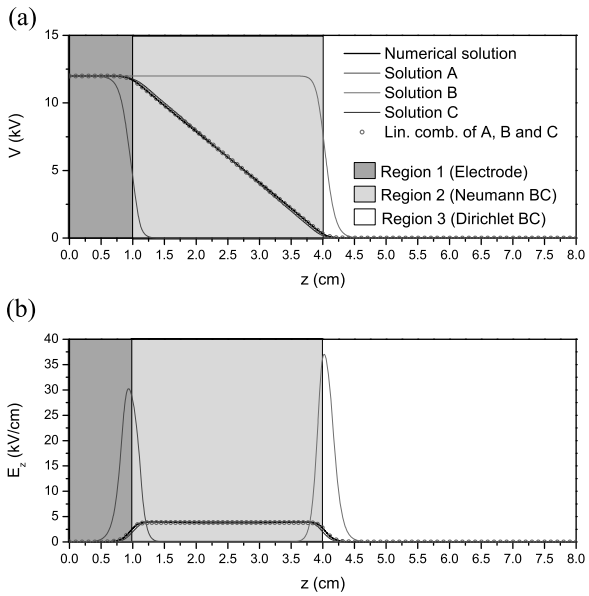

Fig. 4. Distribution of the electric potential (a) and the axial component of the electric field (b) along the axis of the cylindrical geometry. The electrode inner radius is 0.2 cm and its length is 1 cm. The change between the Neumann and the Dirichlet boundary conditions is prescribed at 4 cm from the origin.

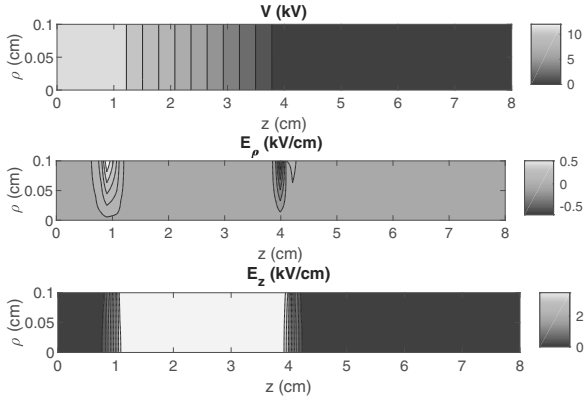

Fig. 5. Contours of the electric potential (a), the radial component of the electric field (b) and the axial component of the electric field (c). The electrode inner radius is 0.2 cm and its length is 1 cm. The change between the Neumann and the Dirichlet boundary conditions is prescribed at 4 cm from the origin.

for solution B and 0.94 for solution C in this case as well, confirming the fact that geometries with proportional dimensions have the same coefficients.

A general comment, based on the evaluation of the change in the linear combination coefficients among the different geometries that have been examined, is that, as the radius of the electrode decreases, the contributions of solutions A and B become less significant. This is evident from the first two geometries that were studied, where the reduction in the electrode inner radius from 0.4 cm to 0.2 cm resulted in an increase of the weight of solution C from 0.94 to 0.96. To further assess this trend, we examined the geometry with an electrode inner radius of 0.1 cm. As expected, the weight of solution C increased to 0.98 at the expense of solutions A and B, wherein their coefficients were both 0.01. The trend is the same when the axial lengths are increased for a constant

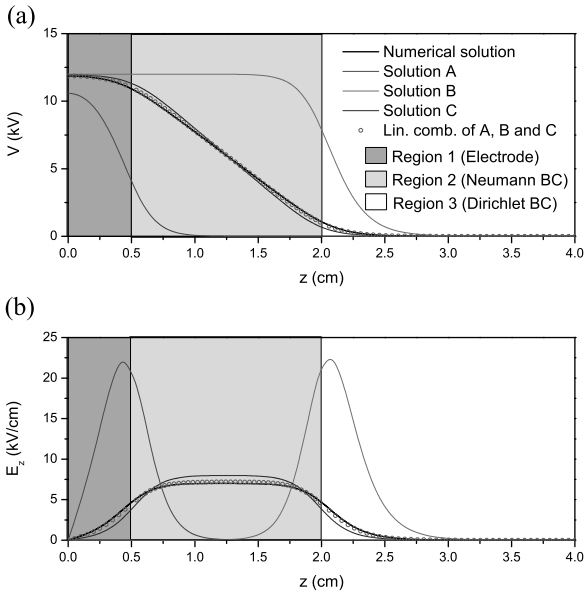

Fig. 6. Distribution of the electric potential (a) and the axial component of the electric field along the axis of the cylindrical geometry (b). The electrode inner radius is 0.4 cm and its length is 0.5 cm. The change between the Neumann and the Dirichlet boundary conditions is prescribed at 2 cm from the origin.

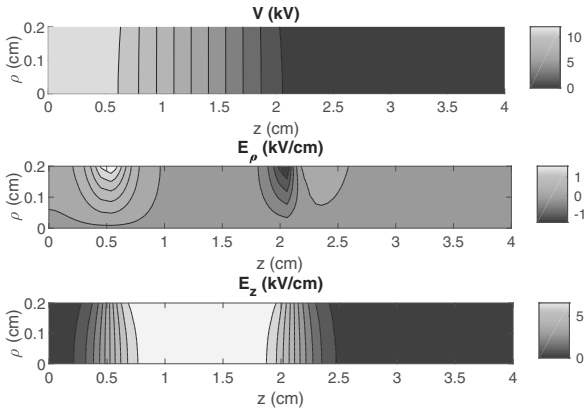

Fig. 7. Contours of the electric potential (a), the radial component of the electric field (b) and the axial component of the electric field (c). The electrode inner radius is 0.4 cm and its length is 0.5 cm. The change between the Neumann and the Dirichlet boundary conditions is prescribed at 2 cm from the origin.

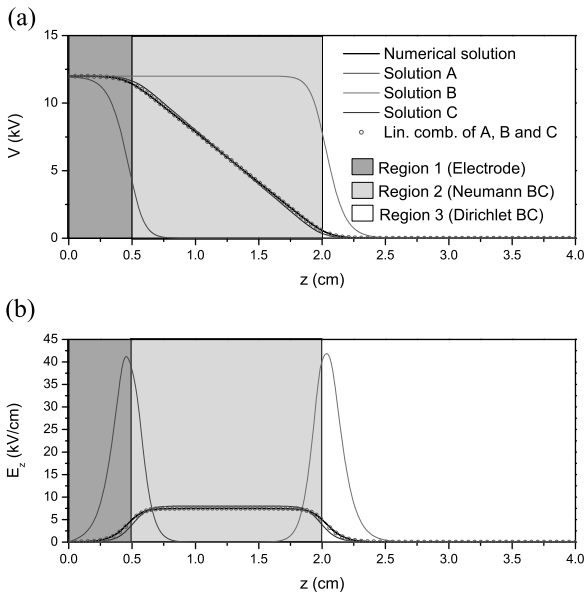

Fig. 8. Distribution of the electric potential (a) and the axial component of the electric field along the axis of the cylindrical geometry (b). The electrode inner radius is 0.2 cm and its length is 0.5 cm. The change between the Neumann and the Dirichlet boundary conditions is prescribed at 2 cm from the origin.

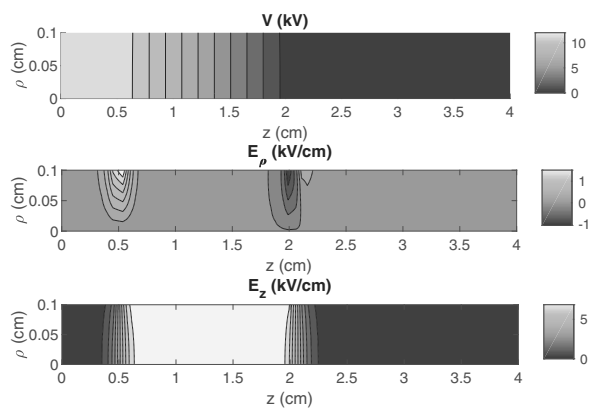

Fig. 9. Contours of the electric potential (a), the radial component of the electric field (b) and the axial component of the electric field (c). The electrode inner radius is 0.2 cm and its length is 0.5 cm. The change between the Neumann and the Dirichlet boundary conditions is prescribed at 2 cm from the origin.

electrode inner radius. It is probable that these three coefficients have a dependence on the three parameters of the geometry, namely, the radius and the length of the electrode and the position where the transition from Neumann to Dirichlet is prescribed. An important role is played by the location of the boundary between Region 2 and Region 3, which is a mathematical approximation and is not based on the geometry of the physical system, i.e., the electrode-dielectric tube configuration.

5. Conclusions

The current research was focused on the presentation of a semi-analytical solution of a mixed-type boundary-value problem, related to the evaluation of the electrostatic potential and the electric field in DBD-based cold plasma jets. The presented model concerned a single biased electrode configuration with different dimensions and it was based on the construction of a three-region domain within a gaseous phase. The contribution of the dielectric tube to the field was neglected, as a fair approximation, based on physical argumentation, although it could affect the electrostatic potential and the produced electric field.

The solution technique for harmonic electrostatic potentials was based on the method of separation of variables of Laplace's equation in the cylindrical coordinate system, which was introduced as the best fitted geometry to the problem. The developed mathematical analysis led to elliptic-type boundary-value problems with either the Dirichlet or the Neumann boundary conditions, accompanied by the vanishing behaviour of the fields at infinity. Therein, apart from the standard terms that were based on the cylindrical harmonic eigenfunctions, the formulae included the contribution of two linear terms that satisfy Laplace's equation *a priori*. In fact, three formulations of the solution were produced, one of which depended only on the exponential terms, the second one included the contribution of the constant term and the third one incorporated both the constant and the linear terms.

The results were compared with a numerical, reference solution of the same physical problem. The plotting of the electrostatic potential and of the electric field of the three formulations of the solution revealed that each variant has different characteristics. This observation was helpful in determining a linear combination of the three formulations that, potentially, can be utilized to produce a unified solution. However, the coefficients of the linear combination depend on the geometric characteristics of the problem, rendering the formulation of a unified solution difficult. Despite the adversities, this is left for future research works.

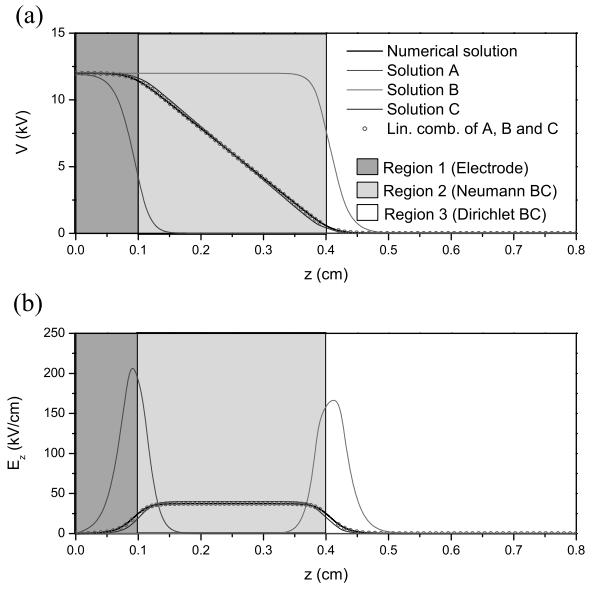

Fig. 10. Distribution of the electric potential (a) and the axial component of the electric field (b) along the axis of the cylindrical geometry. The electrode inner radius is 0.04 cm and its length is 0.1 cm. The change between the Neumann and the Dirichlet boundary conditions is prescribed at 0.4 cm from the origin.

References

Athanasopoulos, D.K., Svarnas, P. and Gerakis, A. (2019). Cold plasma bullet influence on the water contact angle of human skin surface, *Journal of Electrostatics* **102**(103378): 1–12.

Athanasopoulos, D., Svarnas, P., Ladas, S., Kennou, S. and Koutsoukos, P. (2018). On the wetting properties of human stratum corneum epidermidis surface exposed to cold atmospheric-pressure pulsed plasma, *Applied Physics Letters* **112**(213703): 1–5.

Bartecki, K. (2020). Approximate state-space and transfer function models for 2x2 linear hyperbolic systems with collocated boundary inputs, *International Journal of Applied Mathematics and Computer Science* **30**(3): 475–491, DOI: 10.34768/amcs-2020-0035.

Clément, F., Svarnas, P., Marlin, L., Gkelios, A. and Held, B. (2011). Atmospheric-pressure plasma microjet of argon-nitrogen mixtures directed by dielectric flexible tubes, *IEEE Transactions on Plasma Science* **39**: 2364–2365.

Gazeli, K., Svarnas, P., Held, B., Marlin, L. and Clément, F. (2015). Possibility of controlling the chemical pattern of He and Ar "guided streamers" by means of N_2 or O_2 additives, *Journal of Applied Physics* **117**(093302): 1–13.

Gazeli, K., Svarnas, P., Vafeas, P., Papadopoulos, P.K., Gkelios, A. and Clément, F. (2013). Investigation on streamers propagating into a helium jet in air at atmospheric pressure: Electrical and optical emission analysis, *Journal of Applied Physics* **114**(103304): 1–12.

Gkelios, A., Svarnas, P., Clément, F. and Spyrou, N. (2011). Guided propagation of excited species produced by

microjet plasma, *IEEE Transactions on Plasma Science* **39**: 2296–2297.

Gugat, M. and Wintergerst, D. (2018). Transient flow in gas networks: Traveling waves, *International Journal of Applied Mathematics and Computer Science* **28**(2): 341–348, DOI: 10.2478/amcs-2018-0025.

Hobson, E. (1965). *The Theory of Spherical and Ellipsoidal Harmonics*, Chelsea Publishing Company, New York.

Jackson, J.D. (1998). *Classical Electrodynamics*, 3rd Edn, John Wiley & Sons, New York.

Logothetis, D.K., Papadopoulos, P.K., Svarnas, P. and Vafeas, P. (2016). Numerical simulation of the interaction between helium jet flow and an atmospheric-pressure "plasma jet", *Computers and Fluids* **140**: 11–18.

Maksimov, V.I. and Mordukhovich, B.S. (2017). Feedback design of differential equations of reconstruction for second-order distributed parameter systems, *International Journal of Applied Mathematics and Computer Science* **27**(3): 467–475, DOI: 10.1515/amcs-2017-0032.

Moon, P. and Spencer, D.E. (1971). *Field Theory Handbook*, Springer, Berlin/Heidelberg.

Papadopoulos, P.K., Athanasopoulos, D., Sklias, K., Svarnas, P., Mourousias, N., Vratsinis, K. and Vafeas, P. (2019). Generic residual charge based model for the interpretation of the electrohydrodynamic effects in cold atmospheric pressure plasmas, *Plasma Sources Science and Technology* **28**(065005): 1–17.

Papadopoulos, P.K., Vafeas, P., Svarnas, P., Gazeli, K., Hatzikonstantinou, P.M., Gkelios, A. and Clément, F. (2014). Interpretation of the gas flow field modification induced by guided streamer ('plasma bullet') propagation, *Journal of Physics D: Applied Physics* **47**(425203): 1–16.

Popov, N., Babaeva, N. and Naidis, G. (2019). Recent advances in the chemical kinetics of non-equilibrium plasmas, *Journal of Physics D: Applied Physics* **52**(160301): 1–6.

Rabenstein, R. and Trautmann, L. (2003). Towards a framework for continuous and discrete multidimensional systems, *International Journal of Applied Mathematics and Computer Science* **13**(1): 73–85.

Sneddon, I.N. (1966). *Mixed Boundary Value Problems in Potential Theory*, North-Holland Publishing Company, New York.

Svarnas, P., Gazeli, K., Gkelios, A., Amanatides, E. and Mataras, D. (2018a). On the reliable probing of discrete 'plasma bullet' propagation, *Measurement Science and Technology* **29**(045016): 1–9.

Svarnas, P., Matrali, S.H., Gazeli, K., Aleiferis, S., Clément, F. and Antimisiaris, S.G. (2012). Atmospheric-pressure guided streamers for liposomal membrane disruption, *Applied Physics Letters* **101**(264103): 1–5.

Svarnas, P., Matrali, S.H., Gazeli, K. and Antimisiaris, S.G. (2015). Assessment of atmospheric-pressure guided streamer (plasma bullet) influence on liposomes with different composition and physicochemical properties, *Plasma Processes and Polymers* **12**: 655–665.

Svarnas, P., Papadopoulos, P.K., Athanasopoulos, D., Sklias, K., Gazeli, K. and Vafeas, P. (2018b). Parametric study of thermal effects in a capillary dielectric-barrier discharge related to plasma jet production: Experiments and numerical modelling, *Journal of Applied Physics* **124**(064902): 1–13.

Svarnas, P., Papadopoulos, P.K., Vafeas, P., Gkelios, A., Clément, F. and Mavon, A. (2014). Influence of atmospheric pressure guided streamers (plasma bullets) on the working gas pattern in air, *IEEE Transactions on Plasma Science* **42**: 2430–2431.

Svarnas, P., Spiliopoulou, A., Koutsoukos, P.G., Gazeli, K. and Anastassiou, E.D. (2019). Acinetobacter baumannii deactivation by means of DBD-based helium plasma jet, *Plasma* **2**: 77–90.

Vafeas, P., Papadopoulos, P.K., Vafakos, G.P., Svarnas, P. and Doschoris, M. (2020). Modelling the electric field in reactors yielding cold atmospheric–pressure plasma jets, *Scientific Reports* **10**(5694): 1–15.

Weller, H. G., Tabor, G., Jasak, H. and Fureby, C. (1998). A tensorial approach to computational continuum mechanics using object-oriented techniques, *Computers in Physics* **12**(6): 620–631.

Panayiotis Vafeas was admitted to the Department of Chemical Engineering of the University of Patras in 1992 and completed his studies in 1997, with a diploma in chemical engineering. In 2003 he completed his postgraduate studies in the same department, acquiring a postgraduate diploma in simulation, optimization and process control and obtaining a PhD after completing his dissertation. In 2006 he was elected a lecturer at the Department of Engineering Sciences of the University of Patras, and in 2011 he became an assistant professor there. In 2013 he moved to the Department of Chemical Engineering of the University of Patras and in 2015 his position as an assistant professor of the Department of Chemical Engineering of the University of Patras became permanent, while in 2019 he became an associate professor there, a post he holds today. His research activity mainly concerns mathematical modeling of physical problems of mathematical and technological interest with applications in various areas of physics and engineering, such as fluid mechanics, magnetohydrodynamics, electromagnetism, elasticity and plasma theory, but also in the wider area of medical biology, such as magnetoencephalography, electroencephalography and the development of cancerous tumors.

Polycarpos K. Papadopoulos first graduated from the Department of Mechanical Engineering and Aeronautics of the University of Patras. In 2004 he received his PhD degree from the Department of Engineering Sciences there. In September 2013 he joined the Department of Mechanical Engineering and Aeronautics of the University of Patras. His research interests include numerical methods, simulation tools and algorithms.

Panagiotis Svarnas holds a professorial tenure post at the Department of Electrical and Computer Engineering of the University of Patras (Greece). He is also a consultant for national and international companies. His specialty is high voltage engineering, electrical discharges, and cold plasma physics and technology. He has been trained in the University of Patras (Greece) (MSc and PhD in electrical and computer engineering), in the University of Pau et des Pays de l'Adour (France) (PhD in plasma physics with the highest honor), École Polytechnique (France) (2-year research associate), the National Center of Scientific Research (CNRS/Alcatel) of France (1-year research associate), the University of Liverpool (UK) (2-year research associate) and the University of Princeton (USA) (1-year sabbatical visiting professor). Doctor Svarnas has been recognized by the Greek Ministry of National Defense for his scientific excellence in foreign research institutes.

Received: 24 November 2020
Revised: 13 March 2021
Accepted: 5 April 2021